Environmental Science and Pollution Research (2023) 30:46574–46586
https://doi.org/10.1007/s11356-023-25477-9

RESEARCH ARTICLE

Characteristic analysis of s-Fe/Cu two-component micro-electrolysis materials and degradation of dye wastewater

Xiaosen Du[1] · Jin Liu[1,2] · Qing Liu[1] · Guiju Li[1,2] · Yongqing Jiang[1] · Yaxin Zhang[1]

Received: 11 October 2022 / Accepted: 17 January 2023 / Published online: 31 January 2023

Abstract

Micro-electrolysis is a pretreatment technology for difficult-to-biodegrade wastewater. In this study, a chemical displacement method was used to load copper on the surface of sponge iron (s-Fe), and then it was mixed with activated carbon and other components to obtain a multi-element micro-electrolytic filler (OMEF). Through BET, SEM, XRD, XPS, and FT-IR characterization and analysis, OMEF was proved to have a specific surface area of 88.374 m^2/g, C–C, C–O, C = O, O–C = O, and other functional groups and Fe_3C, MnO_2 and other active materials. The removal mechanism of organic pollutants in wastewater by OMEF could be due to the galvanic reaction, direct reduction of Fe, oxidation of Fe, catalytic oxidation of Cu and Mn, and co-precipitation of adsorption. The coupling of the micro-electrolysis and biological methods proved that OMEF had excellent application efficiency. The results indicated that the COD removal rates of OMEF and commercial fillers reached 88.39% and 48.02%, respectively, and the B/C reached 0.74 and 0.3. OMEF showed a better performance. The reusability of the OMEF filler was measured to ensure that the B/C was maintained at around 0.5 during 5 cycles. Kinetic analysis showed that the degradation data of methyl orange (MO) and the removal data of COD obeyed pseudo-second-order kinetics. Moreover, it can further broaden the pH range of treated wastewater and increase the oxidation rate. This new strategy has brought potential enlightenment for the development of high-efficiency wastewater pretreatment using new micro-electrolysis materials. The excellent performance of OMEF micro-electrolytic filler in pretreatment indicated its potential for industrial application.

Keywords s-Fe/Cu bimetal · Micro-electrolysis · Catalysis · Dye · Degradation mechanism · Sponge iron

Responsible Editor: Weiming Zhang

Highlights
- Broaden the pH applicable range.
- The high methyl orange removal rate and CODremoval rate were 87.5% and 87.0%.
- OMEF to B/C improved to 0.74, compared to 0.3for commercial fillers.
- The microbial verification test showed that OMEFhad excellent application performance.
- Synergistic effects of direct reduction of Fe0,oxidation of Fe0, oxidation of Cu0, catalysis by Mn oxides, and adsorption andco-precipitation.

Xiaosen Du and Jin Liu contributed equally to this work.

✉ Guiju Li
liguij@tust.edu.cn

[1] College of Marine and Environmental Sciences, Tianjin University of Science & Technology, Tianjin 300457, People's Republic of China

[2] Key Laboratory of Marine Resource Chemistry and Food Technology (TUST), Ministry of Education, Tianjin 300457, People's Republic of China

Introduction

Azo dye is a commonly used coloring agent. The structure of this type of dye contains one or more molecules of chromophore –N = N– (Basharat and Yasmin 2022, Cui et al. 2021, Sun et al. 2022). These dyes have a very stable structure due to aromatic and conjugated electron systems (Huszánk et al. 2021). Methyl orange (MO) is a widely used anionic azo dye and has been proven to be carcinogenic (Ali et al. 2022; Karimi-Maleh et al. 2022; Khaled et al. 2022; Pete et al. 2021). The persistence and bioaccumulation of these substances increase their potential risks to the environment and human health.

Because of the poor biodegradability of dye wastewater, the pollutant removal efficiency of a separate biochemical process is low. A pretreatment process is required to increase the BOD_5/COD (B/C) value, reduce biological toxicity, and improve the biochemical treatment efficiency of dye wastewater. At present, the developed pretreatment methods

include advanced oxidation methods (AOPs), electrocoagulation, adsorption, and electrochemical oxidation. However, these methods are generally limited by the high cost of functional materials, resulting in an increase in wastewater treatment cost and energy demand (Goncalves et al. 2012; Kishor et al. 2021; Ravinuthala et al. 2022; Yu et al. 2022). Among many pretreatment technologies, micro-electrolysis technology has attracted much attention due to its simple, effective, and green characteristics (Ge et al. 2019; Li et al. 2017a; Rubeena et al. 2018; Segura et al. 2013; Wang et al. 2018). It is the preferred technology for the pretreatment of the highest-concentration and most difficult-to-treat wastewater (Han et al. 2019; Wang et al. 2016). However, the processing efficiency of traditional iron-carbon micro-electrolysis technology is relatively low, and the B/C value is limited. It is usually only suitable for acidic wastewater (Liu et al. 2021; Peng et al. 2021). To improve the oxidation rate of micro-electrolysis, more and more researchers are turning their attention to catalytic micro-electrolysis technology (Liu et al. 2018b). Doping aggregated metal synthesis with bimetallic particles such as Ag, Pd, and Au on zero-valent iron (ZVI) can significantly improve the degradation efficiency of polluting substances (Gao et al. 2019; Gong et al. 2019; Luo et al. 2010; Qiang et al. 2013). However, these precious metals are expensive. Therefore, it is very difficult to put these precious metals to apply widely in industry. In contrast, copper is cheap and has been shown to accelerate the corrosion rate of iron and improve the efficiency of the removal of pollutants (Fang et al. 2018, Xu et al. 2005, Yamaguchi et al. 2018, Zheng et al. 2009).

Sponge iron (s-Fe) is a mixture prepared by reducing iron scales (iron oxide sheet) by carbon reduction below the melting temperature (Xie et al. 2021). Because of its porous, rough surface, and loose spongy shape, s-Fe has been applied to the study of micro-electrolysis (Si et al. 2020; Zhang et al. 2019). Ma et al. (2019a) used s-Fe and activated carbon particles to treat industrial wastewater, and eventually increased the B/C value of industrial wastewater from 0.07 to 0.49. The specific surface area of s-Fe can reach 80 m^2/g, which is far greater than the specific surface area of ordinary zero-valent iron materials (the specific surface area of iron filings and iron powder is about 0.1 ~ 2 m^2/g). The cost of s-Fe is much lower than that of traditional anode materials. Therefore, the choice of s-Fe as the raw material for micro-electrolytic fillers has more market advantages.

In this study, taking full advantage of the large specific surface area of s-Fe, a chemical substitution method was used to load copper onto the surface and internal holes of s-Fe, and s-Fe/Cu bimetallic particles were prepared. Then it was mixed with $MnCO_3$, activated carbon powder, etc. to prepare a new multi-element micro-electrolysis material (OMEF). $MnCO_3$ was chosen because it breaks down into CO_2 and MnO_2 during roasting. CO_2 increases the pore structure inside the filler, which is conducive to providing more reactive sites for the pollutants. And MnO_2 is an efficient catalyst (Alwadai et al. 2023; Panimalar et al. 2022). The filler integrates multiple systems, such as Fe-Cu, Fe–C, Cu-C, and Fe-Fe_3C, to effectively pretreat azo dye wastewater. This paper focuses on the feasibility of the new OMEF by BET, SEM, XRD, XPS, and FTIR and its degradation efficiency in MO-simulated wastewater. The effects of reaction time, initial pH, OMEF dosage, and reuse of wastewater pretreatment were investigated. A comparison of OMEF and commercial fillers and cyclic experiments are also included. And the possible degradation mechanism was inferred by the component comparison test and the free radical capture test. This micro-electrolysis material (OMEF) can improve the biodegradability of wastewater that is difficult to biodegrade and adapt to a wider range of pH.

Experimental methodology

Materials

$CuSO_4 \cdot 5H_2O$ and NaOH were purchased from Kaimat (Tianjin) Chemical Technology Co., LTD; activated carbon, $C_6H_{12}N_4O_9$, and $C_{14}H_{14}N_3NaO_3S$ were purchased from Tianjin Guangfu Technology Development Co., LTD; $MnCO_3$, Ag_2SO_4, $HgSO_4$, $(NH_4)_2Fe\ (SO_4)_2 \cdot 6H_2O$, and $FeSO_4 \cdot 7H_2O$ were purchased from Tianjin Jiangtian Chemical Technology Co., LTD. $K_2Cr_2O_7$ was purchased from Tianjin Solomon Biotechnology Co., LTD; all the chemicals were of analytical grade. Sponge iron was purchased from Lingsong Water Filtration Co., LTD. Commercial micro-electrolysis fillers were purchased from Shandong Senyang Environmental Technology Co., Ltd.

Preparation of OMEF

Synthesis of s-Fe/Cu bimetallic particles. According to the orthogonal test results, the optimal preparation conditions were determined as s-Fe:Cu:Mn:C = 15:5:1:6.3, calcination temperature 800 °C, and calcination time 120 min. The specific parameters of the orthogonal test are listed in supporting information (SI) Tables S1-S2. According to the element mass ratios of Fe and Cu, s-Fe of 25.42 g and $CuSO_4 \cdot 5H_2O$ of 25 g were respectively weighed. Dissolve $CuSO_4 \cdot 5H_2O$ and fix the volume to 1 L, and then transfer it all to a beaker. Fill the beaker with copper solution with s-Fe. Stir with a glass rod at room temperature. The reaction is considered complete when the solution changes from blue to light yellow. The replacement process for loaded copper was completed within 20 min. In order to ensure a full reaction, we chose 30 min as the response time. The product was vacuum filtered. The solid obtained after suction

filtration was washed with deionized water 2–3 times, and then washed with absolute ethanol 2 times. The solid matter was put into a vacuum oven for vacuum drying to prepare bimetallic particles with a mass ratio of s-Fe:Cu of 3:1. Secondly, material mixing. The s-Fe/Cu bimetallic particles, $MnCO_3$, and activated carbon were fully stirred and mixed by ball milling according to the mass ratio of 20:1:6.3. After adding appropriate deionized water, they were put into the granulator for granulation. Raw balls were round balls with a diameter of 6–8 mm. Finally, high-temperature roasting. The crucible containing raw ball material was placed in a tube furnace. With N_2 as the protective atmosphere, it was roasted at 800 °C for 2 h. In this study, all fillers were soaked in raw water for 48 h before use and used after saturation. The composition of s-Fe is listed in Table S3. In order to verify the presence of Cu on s-Fe, XRD and XPS were performed on the samples loaded with Cu. The analysis results are shown in Fig. S1.

Characterization methods

The specific surface area and pore structure of self-made OMEF were analyzed by a specific surface and pore size analyzer (Micromeritics ASAP 2460). The morphology of the synthetic samples was observed by scanning electron microscopy (SEM, jsm-it300lv). To determine the crystallinity of the samples, an X-ray diffractometer patterns were obtained using a scintillation counter (Bruker ADVANCE) with a Cu K radiation source (=0.15406 nm) and recorded from 5 to 80° (2θ) at a scanning rate of 2°/min. Fourier transform infrared (FT-IR) spectra were recorded with a Nicolet 6700 FT-IR spectrometer using KBr pellets.

Degradation test of MO

The laboratory's existing agents are prepared with MO-simulated wastewater at concentrations of 200 mg/L, COD concentrations of 280 mg/L, and B/C of 0.18. Adjust the pH (1, 3, 5, 7, 9, 11) of the MO solution with diluted sulfuric acid and sodium hydroxide. Reaction apparatus diagram as shown in Fig. S2. The acrylic column was filled with a certain amount of fillers (one-time dosage of 50 g/L, 100 g/L, 150 g/L, 200 g/L, 250 g/L) and a fixed pH of simulated wastewater. Aeration was performed at the bottom for the MO degradation test. According to the existing literature, the aeration rate was selected as 1 L/min (Ma et al. 2019). At a specific time, MO solution samples were immediately alkalized for subsequent analysis. The use of micro-electrolytic materials will dissolve trace iron ions, copper ions, and so on. As a result, the methyl orange solution is alkalized in order to precipitate the metal ions in the sample, and the final liquid is obtained through filtration.

Kinetic analysis

To investigate the degradation kinetics, the pseudo-second kinetics model was used for data fitting, and the kinetic expression can be presented as follows:

$$\frac{1}{C_t} = \frac{1}{C_0} + k_{obs}t \tag{1}$$

where C_t is the concentration of MO or COD at time t, C_0 is the initial concentration of MO or cod, k_{obs} (min^{-1}) is the secondary degradation rate constant, and t is the reaction time.

Analytical methods

Each set of experiments was performed at least twice, with experimental data averaged. When the deviation of the two sets of data was greater than 5%, the 3rd trial was performed to take the average. MO concentration was measured with an ultraviolet–visible spectrophotometer (TU 1810). The determination of COD concentration was performed by potassium dichromate titration (HJ828-2017). The atomic absorption spectrophotometer (AA-7003F) is used for the determination of iron and copper ion concentrations. Differential pressure direct-reading BOD determination device (CY-2) for BOD_5 concentration analysis. The pH is determined with an acidity meter (RL 150).

Results and discussion

Characteristics of OMEF before and after the reaction

BET analysis of OMEF

To a certain extent, the micro-electrolytic properties of OMEF are related to its specific surface area and pore structure. The specific surface area of OMEF was measured by the specific surface area and pore size analyzer as 88.374 m^2/g, the total pore volume was about 0.059 cm^3/g, and the average pore size was 3.816 nm, which belonged to the medium pore (2–50 nm) range. Figure 1 shows the N_2 adsorption/desorption isotherm of OMEF. The hysteresis loop can be observed in the figure.

The inset in Fig. 1 was the BJH pore size distribution curve of OMEF. It can be seen from the figure that most of the pore size of the self-made filler was distributed in the mesopore range. The specific surface area of OMEF was much larger than that of commercially available iron-carbon fillers (Liu et al. 2018, Peng et al. 2021).

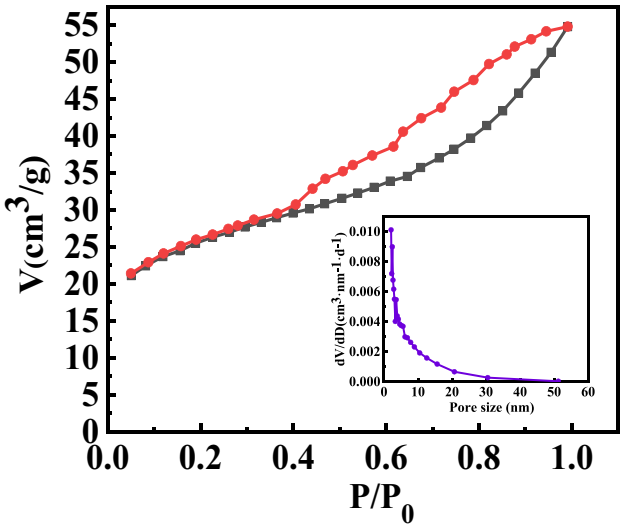

Fig. 1 N_2 adsorption/desorption isotherm of OMEF; (inset) BJH aperture distribution of OMEF

SEM analysis of the fresh and used OMEF

Figure 2a, b and c, d show the topographic characteristics of the filler before and after use, respectively. It can be seen that the surface of the filler had a microstructure before use, providing a suitable position for the reaction. The surface of the filler after the reaction was rougher, which may be caused by the corrosion of iron during the reaction or the organic matter adsorbed on the surface of the filler. This phenomenon was consistent with the results of existing studies (Zhao et al. 2021).

XRD analysis of the fresh and used OMEF

XRD analysis of OMEF before and after use was shown in Fig. 3. The main components of OMEF before use were Fe^0, Cu^0, Cu_2O, CuO, Fe_2O_3, Fe_3O_4, Fe_3C, and MnO_2. Fe^0 was detected at 44.673° of the (1 1 0) plane with cubic spinel structure (PDF# 06–0696). Diffraction peaks 2θ = 43.316°, 50.448°, and 74.124° correspond to Cu^0 in the (1 1 1), (2 0 0), and (2 2 0) planes (PDF# 85–1326). Cu_2O in the (1 1 1) plane was detected at 2θ = 36.59° (PDF# 04–003-6433). The diffraction peak at 2θ = 35.543° corresponds to CuO in the (1 1 − 1) plane (PDF# 048–1548). Fe_2O_3 with hematite and magnetite crystal phases can be detected in OMEF (PDF # 73–0603). The cubic crystal phase Fe_3O_4 can also be detected by XRD (PDF# 75–1372). Although firing was carried out with N_2 as a protective atmosphere, the presence of iron oxides and copper oxides indicated that a series of complex processes occur during high-temperature roasting. This was related to the partial pressure of oxygen in the

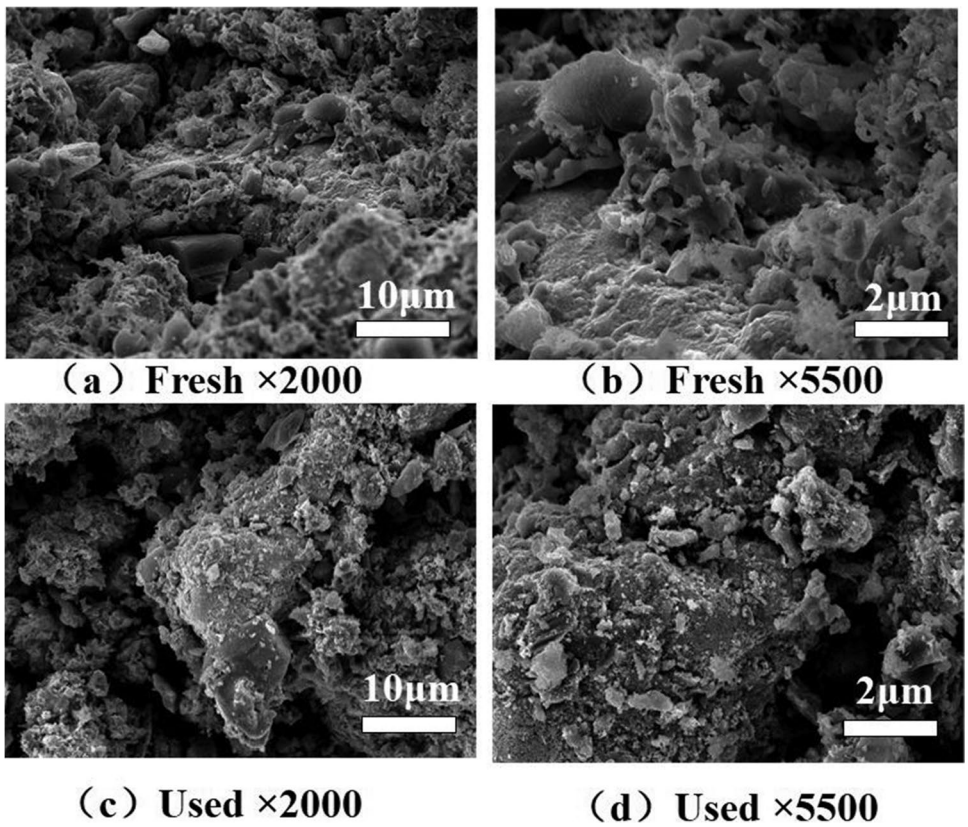

Fig. 2 SEM of OMEF before and after use

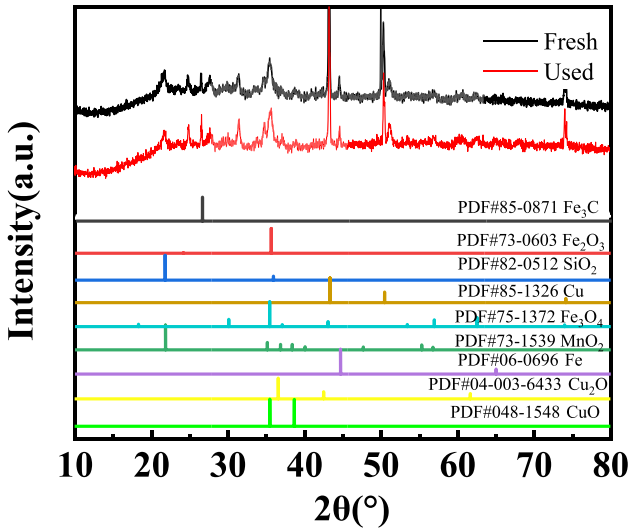

Fig. 3 XRD plots of fresh and used fillers

furnace chamber during the sintering process, and also to the addition of H_2O or other forms of oxygen during the preparation process. Studies (Chakri et al. 2017) had found that Fe_3O_4 as an anode can accelerate electrolytic reactions. Fe_3C (PDF# 85–0871) of the diffraction peak corresponding to the (0 0 2) plane at 2θ = 26.499°. Niu et al. (2019) found that the potential difference between Fe^0 (anode) and Fe_3C (cathode) can also facilitate the progression of micro-electrolytic reactions. Diffraction peak 2θ = 21.807° corresponded to (1 1 0) crystal plane MnO_2 (PDF # 73–1539). The presence of MnO_2 was due to the addition of $MnCO_3$ during preparation. MnO_2 is a good catalyst and semiconductor material that can further improve the degradation efficiency of organic matter in wastewater by micro-electrolytic systems (Alwadai et al. 2023; Chen et al. 2022; Panimalar et al. 2022). In Fig. 3, only the peak value of Cu^0 has a little deviation that is not obvious, while the peak value of other elements does not change. This indicates that the property of OMEF is stable after use.

XPS analysis of the fresh and used OMEF

X-ray photoelectron spectroscopy (XPS) was used to characterize the element composition of the filler and the valence states of O, C, Fe, Cu, and Mn (Fig. 4a–f). The element detection results were in good agreement with the XRD pattern results. According to the peak-splitting plot of Fig. 4b, the OMEF surface before and after the reaction showed three peaks, and the combined energy can be near 530.6, 531.8, and 533.2 eV, which corresponded to lattice oxygen species (O_{lat}), adsorbed oxygen species (O_{abs}) (Paparazzo 2017), and H_2O species, respectively. On the surface of OMEF before and after the reaction, the O_{abs} peak intensity was much higher than the O_{lat} peak intensity, which indicated many oxygen vacancies were present on the surface of the filler. Oxygen vacancies promote the migration of oxygen ions (Wu et al. 2020). The convenient conditions of oxygen ion transport indicate that OMEF also had strong reactivity after use (Wu et al. 2020).

According to C1s peak in Fig. 4c, the binding energy corresponds to C–C, C–O, C = O, and O–C = O at 284.8, 285.5, 288.5, and 289 eV, respectively, compared with the number of functional groups in similar studies (Zhao et al. 2020). C1s peak splitting Fig. 4c shows that the binding energy at 284.8, 285.5, 288.5, and 289 eV correspond to C–C, C–O, C = O, and O–C = O, respectively. Compared with similar studies, the number of functional groups had increased (Xu et al. 2019). The more carbon-related groups, the better the micro-electrolysis performance of the filler. After the reaction, the relative content of C–C decreased from 26.06 to 18.53%. The relative content of O–C = O increased from 4.09 to 6.12%. The relative contents of C–O and C = O changed little. It showed that the micro-electrolysis reaction had little damage to the oxygen-containing functional groups. The fillers involved in the reaction were still highly active.

Figure 4d shows the Fe2p XPS results of fresh and used samples. Two kinds of Fe states are analyzed from Fe2p XPS, which are Fe^{2+} and Fe^{3+}. $Fe2p_{1/2}$ centered on 724.7 eV, $Fe2p_{3/2}$ centered on 710.1 eV, and there is a satellite peak between $Fe2p_{1/2}$ and $Fe2p_{3/2}$ (Miao et al. 2021). The presence of Fe(II) and Fe(III) states on the surface of fresh fillers was demonstrated. Remarkably, compared with unused fillers, the proportion of Fe^{2+} on the surface of the filler after use decreased, and the proportion of Fe^{3+} increased. This indicated that the micro-electrolysis process was accompanied by corrosion and surface oxidation of iron. This phenomenon was consistent with the existing reports (Zhao et al. 2021).

Figure 4e shows the peak spectrum of Cu2p. The high-resolution Cu2p spectrum of metallic copper in Fig. 4e can be deconvoluted into two sharp peaks at binding energies of 932.5 eV and 952.4 eV, which are assigned to the $Cu2p_{3/2}$-$Cu2p_{1/2}$ doublet, respectively (Khalakhan et al. 2021). There are two satellite peaks between $Cu2p_{1/2}$ and $Cu2p_{3/2}$ and to the left of $Cu2p_{1/2}$. The characteristic peaks of Cu^0, Cu^+, and Cu^{2+} were observed at 932.5 eV, 933.2 eV, and 935 eV (Xu et al. 2019). Due to slight surface oxidation of the filler during firing, the Cu^+/Cu^{2+} signal of the fresh filler was detected. This was consistent with the results of the analysis of copper in XRD. The amount of Cu^0 and Cu^+ in the used fillers was significantly reduced, and the amount of Cu^{2+} increased. The conversion of $Cu^0/Cu^+ \rightarrow Cu^{2+}$ was performed (Eqs. (10)–(12)). The results showed that the copper component could assist the iron-based Fenton reaction and promote the removal of MO.

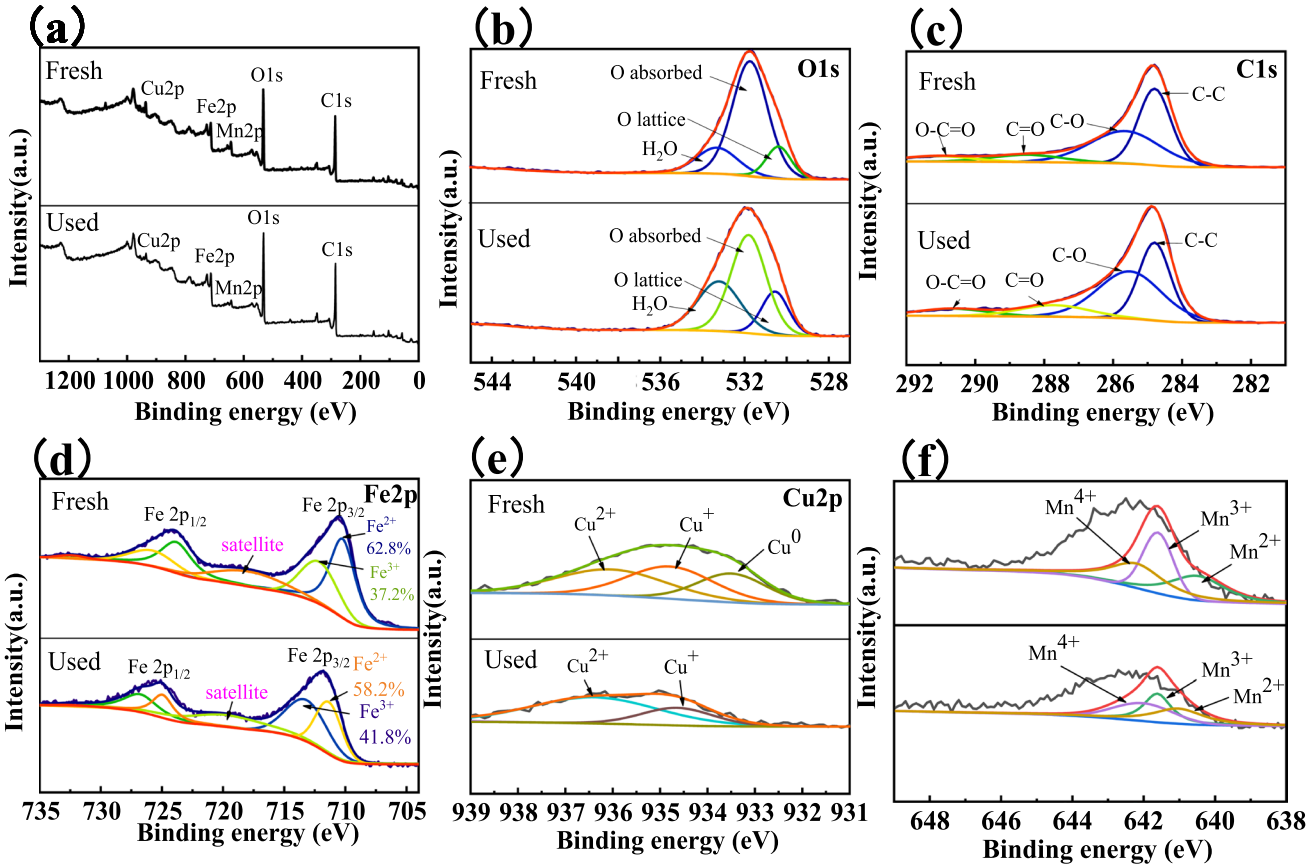

Fig. 4 XPS spectra of fresh and used filler **a** XPS full spectrum; high-resolution XPS **b** O1s; **c** C1s; **d** Fe2p; **e** Cu2p; **f** Mn2p

As shown in Fig. 4f, the peaks of 652.5 and 640.7 eV were considered to belong to $Mn2p_{1/2}$ and $Mn2p_{3/2}$, respectively. There are three strong characteristic peaks, which are Mn^{2+} (640.5 eV), Mn^{3+} (641.6 eV), and Mn^{4+} (642.2 eV) (Cheng et al. 2021). Mn has a thermodynamically favorable redox pair, Mn^{3+}/Mn^{4+}. It can accelerate electron transfer and increase conductivity.

FTIR analysis of the fresh and used OMEF

Figure 5 shows that the wide absorption band observed at 3433 cm^{-1} (Shen et al. 2021) was due to the stretching vibration of the associated hydroxyl group. At 1632.1 cm^{-1} was the peak of the C = O bond. The band at 1090 cm^{-1} corresponds to the C–O telescopic vibration. It was also the fingerprint of the hydroxyl group (Zhao et al. 2021). These oxygenated functional groups facilitate the adsorption of contaminants and enhance the hydrophilicity of the material. 875 cm^{-1} corresponded to the in-plane and out-of-plane deformation vibration of Fe–OH on the surface of goethite. The Fe–O–Fe tensile vibration at 568 cm^{-1} was the characteristic band of iron oxide. The Cu–O stretching vibration at 472.1 cm^{-1}. The absorption band at 967 cm^{-1} was caused by

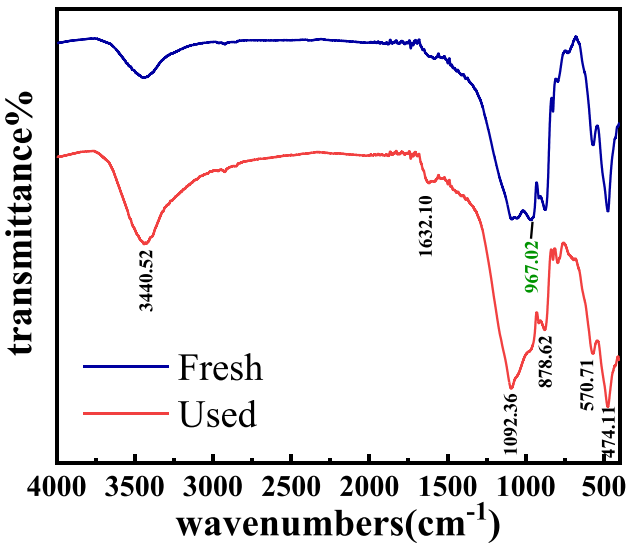

Fig. 5 FTIR spectra of OMEF before and after use

the telescopic symmetrical vibration of O_B–Si–O_B (bridge oxygen). The strength of the absorbing band of the used filler was weakened at 967 cm^{-1}. O_B–Si–O_B group density

reduction and O_T–Si–O_T (non-bridge oxygen) group density increase are the main reasons.

Study on OMEF degradation of dyestuff wastewater

Comparison of treatment effect between OMEF and commercial filler

In this study, the single-factor variable method was used to investigate the effects of reaction time, initial pH, and one-time filler dosage on the degradation of simulated methyl orange wastewater. Finally, the best process parameters were selected: the reaction time was 120 min, the initial pH was 8.26, and the dosage was 150 g/L. And both kinds of fillers are tested under the condition of adsorption saturation to remove the effect of adsorption. See Figs. S3-S5 for the specific screening process. All experimental factors are the same to ensure the scientific nature and accuracy of the experiment.

The commercial filler and OMEF will be used as a control experiment to explore the influence of the two on the COD and B/C of methyl orange simulated wastewater under the same operating parameters. The COD removal rates of the two fillers used to simulate methyl orange wastewater at different pH were shown in Fig. 6a and b.

Figure 6a shows that the COD removal rate of OMEF was better than that of a commercial filler. Further, the COD removal rate of OMEF was 88.39%, while that of a commercial filler was only 48.02%. From the perspective of biodegradability, the B/C of commercial micro-electrolysis materials was only 0.3, and the B/C of effluent treated by OMEF reached 0.74, which significantly improved the biodegradability. Studies had shown (Li et al. 2017b) that the synergistic effect of persulfate Fe–C micro-electrolysis was used to degrade MO, and its B/C value increased to 0.65. Compared with previous studies, the B/C under the condition of no oxidizing agent in this study increased by 0.09, indicating that the self-made fillers in this study had better effects.

Figure 6b shows that both commercially available fillers and OMEF had the best effect when the pH was 3. And the removal rate generally decreased with the increase in pH. This was due to the decrease of H^+ content with the increase of alkalinity and the decrease of [H] generation. However, in the pH range of 5–11, the removal rate of COD by OMEF was about 80%. To further analyze the effect of different pH values, kinetic analysis at different pH values was performed. See Table 1.

Table 1 shows that the reaction rate constant (k_{obs}) values for the degradation of methyl orange at pH 1–5 all reached their maximum at pH = 3. This was due to the fact that zero-valent iron produces more corrosion in lower pH solutions, thereby accelerating the rate of oxidation of contaminants. However, when the pH was low (pH = 1), a large amount of corrosion of s-Fe (Eq. (2)) can cause too much H_2 to cover the OMEF surface (Yu et al. 2017a). The contact between MO and filler was blocked, so the removal rate decreased. The effect on degradation at pH = 5 was not much different from that at pH 7. In the pH range of 7–11, the k_{obs} value gradually decreased. However, in the pH range of 5–11, the removal rate of COD reached more than 80%, which proved that OMEF had better treatment efficiency in a wide pH range. Therefore, the optimal pH value for OMEF treatment of simulated MO wastewater was determined to be pH = 3. However, in order to ensure treatment effect and

Table 1 Pseudo-second-order rate constants of MO degradation over OMEF under different pH

pH	MO removal rate		COD removal rate	
	k_{obs} (min^{-1})	R^2	k_{obs} (min^{-1})	R^2
1	2.7429E − 4	0.9667	4.2482E − 5	0.9439
3	1.1E − 3	0.9301	2.5883E − 4	0.9656
5	2.7116E − 4	0.9698	1.9683E − 4	0.9880
7	3.4473E − 4	0.9688	2.2223E − 4	0.9765
8.26	2.9594E − 4	0.9764	2.1985E − 4	0.9924
9	2.9297E − 4	0.9820	1.8127E − 4	0.9509
11	2.0948E − 4	0.9847	1.4538E − 4	0.9874

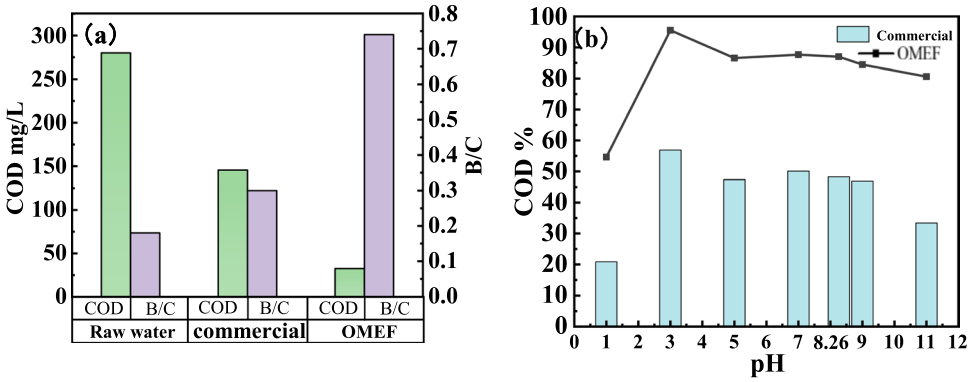

Fig. 6 **a** Raw water and effluent water quality after treatment with different materials; **b** comparison of COD removal by commercial filler and OMEF at different pH

cost savings, the subsequent test did not adjust the pH of the simulated water sample.

$$2H^+ + 2e^- \rightarrow 2[H] \rightarrow H_2 \quad E^0\left(\frac{H^+}{H_2}\right) = 0.00V \tag{2}$$

Micro-electrolysis/biological method

To verify the effect of OMEF filler treatment on the biochemical improvement of dyeing wastewater, micro-electrolysis was combined with the activated sludge method for the degradation test. The dyeing wastewater came from a printing and dyeing factory in Tianjin, and the measured wastewater chromaticity was 5000 times and the COD concentration was 1160 mg/L. The biochemical reaction strains in the experiment were screened, film-mounted, and domesticated by our group. As shown in Fig. 7, the micro-electrolysis effluent was connected to the biochemical tank using a peristaltic pump, and the effluent flow rate was controlled by clamps. The effluent COD concentration was measured at a fixed time.

The effluent from the micro-electrolysis stage using the activated sludge method stabilized after 24 h. The COD concentration was less than 100 mg/L after this time. The colorimetric determination was performed using the dilution multiplier method. The chromaticity of the biochemical stage was 150 times. The chromaticity of the biochemical effluent had not yet reached the standard. Furthermore, after the biochemical effluent is subjected to ozone aeration treatment for 5 min, the chromaticity is close to 10, and the COD concentration is 50 mg/L. The combined use of the microbial method further verified the synergistic effect between the various mechanisms and the high efficiency of OMEF.

Cyclic experiments

Under optimal process parameters, OMEF was tested for reusability. As shown in Fig. 8a and b, within 5 degradation cycles, the removal rates of OMEF to MOs after 120 min of the reaction were 87.5%, 69.5%, 64.5%, 68.3%, and 68.6%, and the removal rates of COD were 87.0%, 78.0%, 74.4%, 67.8%, and 68.4%, respectively. The effect of the filler was reduced significantly after being used once. In the next 4

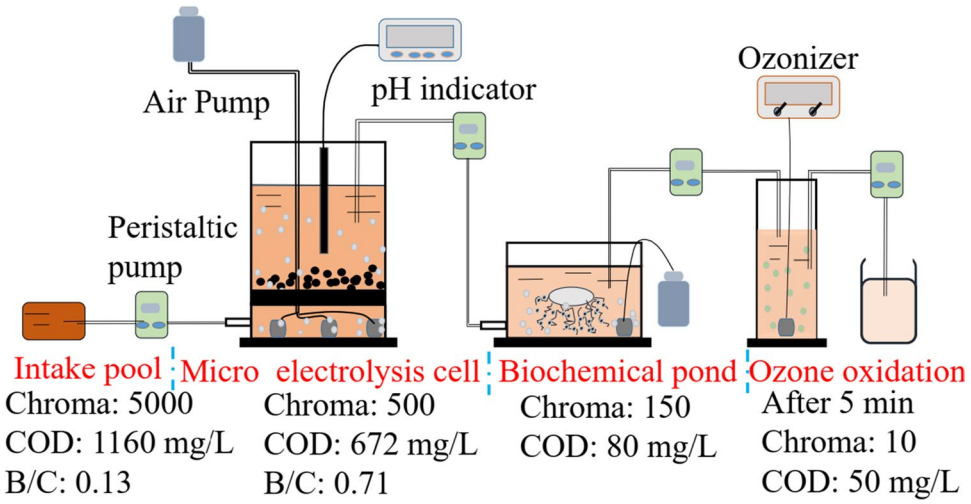

Fig. 7 Micro-electrolysis/biochemical/ozone reaction device diagram

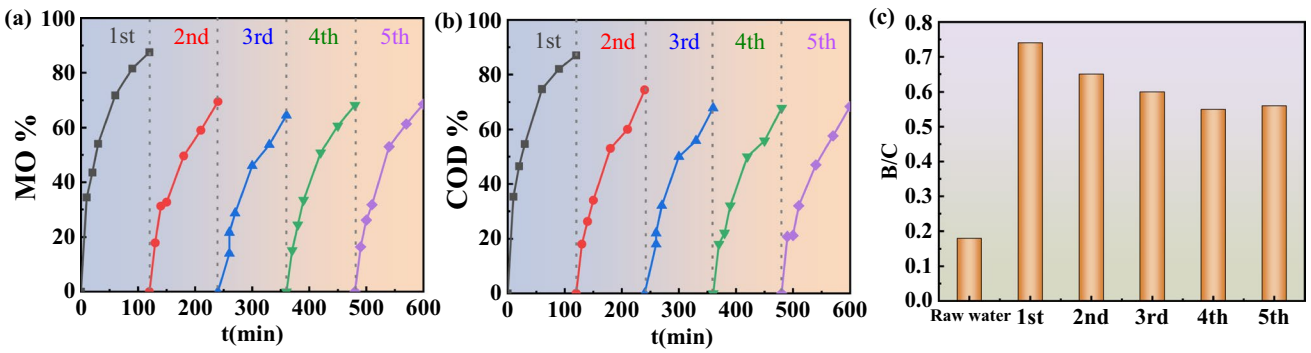

Fig. 8 Different cycle times **a** MO removal; **b** COD removal; **c** B/C values

cycles, the effect reduction did not differ much. This was due to the fact that after 1st cycle, the maximum amount of dissolved iron ions from the filler is 1.46E − 3 mg/g, copper ions were 1.06E − 3 mg/g, and the amount of dissolved manganese ions was closed to 0. In the 2nd–5th cycles, the amount of dissolved iron ions was lower than 1.01E − 3 mg/g, and the amount of dissolved copper and manganese ions was closed to 0. After the first cycle of the filler, the loss of the main active components gradually decreased, and the reaction system gradually stabilized. After that, the filler used 5 times was soaked for 10 days, and the iron ion leaching concentration was 0.067 mg/L, and the amount of loss was very small. As shown in Fig. 8c, the B/C of raw water was 0.18, and the B/C of recycling 1–5 cycles was 0.74, 0.65, 0.60, 0.55, and 0.56, respectively. The self-made filler can greatly improve the biodegradability of the simulated wastewater. After 5 cycles of recycling, B/C remained above 0.5, which proved that the self-made OMEF had good stability. The previous FTIR results also indicate that OMEF has good reusability. The characteristic spectra of fillers before and after use had not changed significantly, which proved good reusability. Therefore, self-made electrolytic fillers had great commercial potential.

Reaction mechanisms

To explore the role of each component in the filler in the reaction process, s-Fe, s-Fe/Cu, s-Fe + C, s-Fe/Cu + C, and s-Fe/Cu + Mn + C were compared tests. By adding absolute ethanol (EtOH) and p-benzoquinone (PBQ) as quenchers for ·OH and $\cdot O_2^-$, respectively, the effects of the two radicals on the degradation of methyl orange were investigated, as shown in Fig. 9a and b.

It can be seen from Fig. 9a that the removal rate of COD was only about 22% when s-Fe was added alone. After adding the Cu element (s-Fe/Cu), the removal rate of COD reached 35%. After adding activated carbon based on s-Fe and s-Fe/Cu, the removal rate of COD was significantly improved, about 57% and 67%, respectively. It can be seen that the addition of Cu and C elements can improve the removal efficiency of COD. More specifically, copper acts as a cathode at a high potential of 0.781 V (Yu et al. 2017b) to have an electrode reaction between iron and copper. In addition, there was a potential difference of 1.2 V between iron-carbon and 0.423 V between copper-carbon and iron. The synergistic effect between Cu, Fe–C, and Cu-C primary cells accelerated the corrosion of s-Fe and the generation of [H]. [H] can break macromolecular chains into small molecular chains, reduce COD, and improve biodegradability. By adding Mn on the basis of s-Fe/Cu + C, the removal rate of COD increased to about 87%. This showed that Mn element also played a promoting role in the micro-electrolysis system. This was due to the addition of $MnCO_3$. On the one hand, the S_{BET} of the filler was increased from 73.51 to 88.37 m^2/g, which can provide a large number of reactive sites; on the other hand, the formed MnO_2 had the effect of catalytic degradation.

The effect of free radicals on the degradation of MO was investigated by adding anhydrous ethanol (EtOH) and p-benzoquinone (PBQ) as quenchers of ·OH and $\cdot O_2^-$, respectively. As shown in Fig. 9b, the addition of either EtOH or PBQ inhibited the degradation of MO. In this experiment, 0.26 mol EtOH and 0.015 mol PBQ were used each time. The degradation of MO decreased from 87.5 to 76.8% and the k_{obs} value decreased from 2.95E − 4 to 1.48E − 4 min^{-1} with the addition of EtOH only. The addition of PBQ decreased the degradation of MO from 87.5 to 38.7% and the k_{obs} value decreased to 2.39E − 5 min^{-1}. The addition of PBQ significantly inhibited the degradation of MO. The co-addition of EtOH with PBQ had the greatest effect on the degradation of MO. The removal rate was only 16.3% and the k_{obs} value decreased to 8.45E − 6 min^{-1}. ·OH and $\cdot O_2^-$ contributed 10.7% and 48.8% to the degradation of MO, respectively. The synergistic effect of ·OH and $\cdot O_2^-$ was observed. The synergistic contribution of both was 71.2%. It was proved that ·OH and $\cdot O_2^-$ played a crucial role in the system of this study.

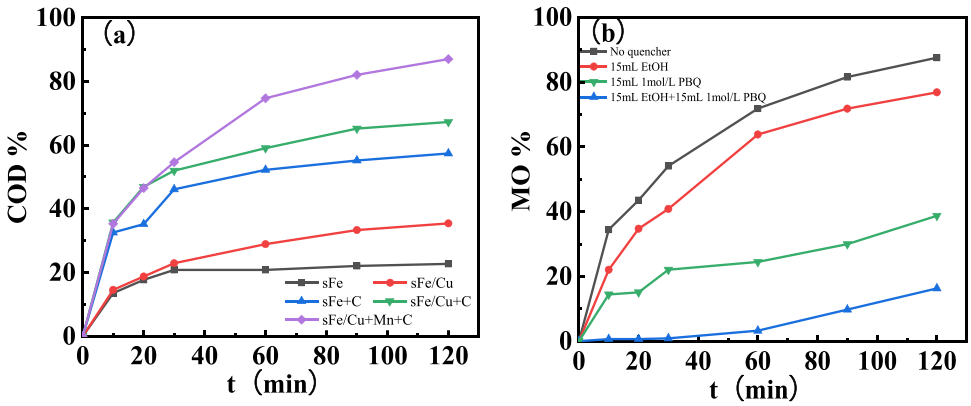

Fig. 9 **a** Micro-electrolysis effect of different components; **b** effect of different quenchers on methyl orange removal

According to the existing test results and literature research in this study, the mechanism of OMEF degradation of methyl orange in this study was finally proposed, as shown in Fig. 10. It mainly includes 4 parts: galvanic cell reaction, direct reduction of Fe to methyl orange, oxidation of Fe, catalytic oxidation of Cu and Mn, adsorption and co-precipitation.

First, Fe and activated carbon can form galvanic cells in the electrolyte solution. The electrode reaction can be presented as follows:

Anode:

$$Fe^0 - 2e^- \rightarrow Fe^{2+} \quad E^0(Fe^{2+}/Fe^0) = -0.44V \tag{3}$$

Cathode (alkaline):

$$O_2 + 2H_2O + 4e^- \rightarrow 4OH^- \quad E^0\left(\frac{O_2}{OH^-}\right) = 0.040V \tag{4}$$

Then, when Cu powder is added to the system, which also can form galvanic cells with activated carbon, the electrode reaction can be presented as follows:

Anode:

$$Cu^0 - 2e^- \rightarrow Cu^{2+} \quad E^0(Cu^{2+}/Cu^0) = +0.34V \tag{5}$$

Cathode (alkaline):

$$O_2 + 2H_2O + 4e^- \rightarrow 4OH^- \quad E^0\left(\frac{O_2}{OH^-}\right) = 0.40V \tag{4}$$

At the same time, there is a potential difference between Fe and Cu, which can form a primary battery.

It can be seen from the above electrode reactions that in multiple micro-electrolysis systems, Fe and C can form microcells, Cu and C can form microcells, and Fe and Cu can form microcells, and Cu has good electrical conductivity, which is conducive to promoting the galvanic cell reaction. In many micro-electrolysis systems, Cu and Fe constitute a bimetallic catalytic system, which improves the efficiency of catalytic degradation reactions.

As the reaction proceeded, the reaction of Eq. (4) occurred in the presence of oxygen. O_2 enhanced the production of hydroxide ions in the micro-electrolytic system. This caused an increase in pH. DO can enhance the generation of hydroxyl ions to form more iron hydroxides. It has been found that the generated iron hydroxide can easily adsorb organic molecules containing electron-donating groups, so plenty of dye molecule was adsorbed and co-precipitated with iron hydroxides. Afterward, Fe performed a direct reduction of MO. Meanwhile, the oxidation of Fe by O_2 can produce H_2O_2 (Eq. (6)). Fe^0 reacted with H_2O_2 to produce Fe^{2+}. Fe^{2+} reacted with H_2O_2 to produce ·OH and Fe^{3+} (Eqs. (7), (8)). Fe^{3+} reacts with Fe^0 to produce Fe^{2+} (Eq. (9)), etc. The presence of Cu^0 will promote the corrosion of Fe^0 to generate more Fe^{2+}, thus promoting oxidation.

After 120 min of reaction, copper ions were detected at a concentration of about 0.16 mg/L. The presence of trace copper ions proved that oxidation by Cu^0 was present in the reaction system. Dissolved oxygen can accept the electrons provided by copper and the Cu^+/Cu^{2+} cycle generated a Fenton-like reaction (Eqs. (10)–(12)). This phenomenon was consistent with the results of XPS analysis. In addition, the K_{sp} of $Cu(OH)_2$ in an aqueous solution was 2.2×10^{-22}, which was higher than that of $Fe(OH)_3$ (4.0×10^{-38}) (Xia et al. 2021), indicating that Cu^{2+} entering the solution can inhibit the formation of the dense passivation layer on the filler surface. Therefore, the active component inside the

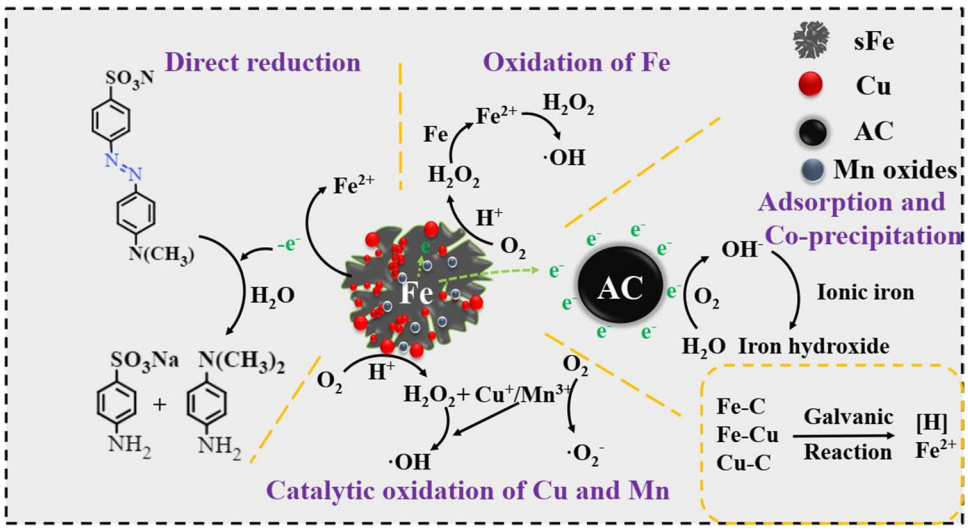

Fig. 10 Mechanism of degradation of MO by OMEF

filler can be continuously exposed to promote the oxidative degradation of MO, which makes OMEF more reusable. In addition, the Mn^{3+}/Mn^{4+} cycle also generated a Fenton-like reaction (Eqs. (13)–(15)), which promoted the reaction activity.

$$Fe^0 + O_2 + 2H^+ \rightarrow Fe^{2+} + H_2O_2 \quad (6)$$

$$Fe^0 + H_1O_2 \rightarrow Fe^{2+} + 2OH^- \quad (7)$$

$$Fe^{2+} + H_2O_2 \rightarrow Fe^{3+} + \cdot OH + OH^- \quad (8)$$

$$Fe^0 + Fe^{3+} \rightarrow Fe^{2+} \quad (9)$$

$$O_2 + 2H^+ + 2Cu^0 \rightarrow H_2O_2 + 2Cu^+ \quad (10)$$

$$Cu^+ + O_2 \rightarrow Cu^{2+} + \cdot O_2^- \quad (11)$$

$$H_2O_2 + Cu^+ \rightarrow Cu^{2+} + \cdot OH + OH^- \quad (12)$$

$$O_2 + 2H^+ + 2Mn^{2+} \rightarrow H_2O_2 + 2Mn^{3+} \quad (13)$$

$$Mn^{3+} + O_2 \rightarrow Mn^{4+} + \cdot O_2^- \quad (14)$$

$$H_2O_2 + Mn^{3+} \rightarrow Mn^{4+} + \cdot OH + OH^- \quad (15)$$

Conclusions

A multifaceted micro-electrolytic catalytic material was successfully synthesized and characterized by BET and SEM to show a rich pore structure with a large specific surface area. This can provide a large number of active sites for the reaction. The fillers were characterized by XRD, XPS, and FTIR, which proved that OMEF contains more active substances and functional groups than before. It also showed that the filler still had high activity after use. The OMEF could adapt to a wide pH range. The experimental process was consistent with the pseudo-second kinetics model. In addition, when compared to commercially available fillers, OMEF improved the B/C value of wastewater from 0.18 to 0.74, while commercially available fillers only improved to 0.3. The cyclic experiment results showed that the B/C remained above 0.5 after 5 times of OMEF recycling. It proved that the OMEF had good stability. The results of coupled micro-electrolysis/biological method showed that the OMEF could provide better treatment conditions for the biochemical stage. Through the quenching test, characterization results, and comprehensive analysis of the experimental results, the reaction was presumably determined to include five degradation mechanisms, which were the galvanic reaction, direct reduction of Fe, oxidation of Fe, catalytic oxidation of Cu and Mn, and co-precipitation of adsorption.

Supplementary Information The online version contains supplementary material available at https://doi.org/10.1007/s11356-023-25477-9.

Author contribution Xiaosen Du: conceptualization, data curation, formal analysis, methodology, software, visualization, writing—original draft. Jin Liu: conceptualization, data curation, methodology, software, writing—original draft. Qing Liu: writing—review and editing. Guiju Li: conceptualization, data curation, formal analysis, funding acquisition, methodology, project administration, resources, writing—review and editing. Yongqing Jiang: investigation. Yaxin Zhang: investigation.

Funding This project was supported by the National Natural Science Foundation of China (Grant No. 22006112); Tianjin Natural Science Foundation (Grant No. 20JCQNJC00060); and Ministry of Science and Technology SME Innovation Fund Project (Grant No. 10C26211200185).

Data availability The datasets used during this study are available from the authors on reasonable request.

Declarations

Ethical approval Not applicable.

Consent to participate Not applicable.

Consent for publication Not applicable.

Competing interests The authors declare no competing interests.

References

Ali SS, Al-Tohamy R, Sun J (2022) Performance of Meyerozyma caribbica as a novel manganese peroxidase-producing yeast inhabiting wood-feeding termite gut symbionts for azo dye decolorization and detoxification. Sci Total Environ 806:150665. https://doi.org/10.1016/j.scitotenv.2021.150665

Alwadai N, Manzoor S, Huwayz MA, Abdullah M, Khosa RY, Aman S, Abid AG, Alrowaili ZA, Al-Buriahi MS, Farid HMT (2023) Facile synthesis of transition metal oxide SnO2/MnO2 hierarchical nanostructure: as an efficient electrocatalyst for robust oxygen evolution reaction. Surf Interfaces 36https://doi.org/10.1016/j.surfin.2022.102467

Basharat Z, Yasmin A (2022) Sulphonated azo dye decolorization by Alcaligenes faecalis subsp. phenolicus MB207: insights from laboratory and computational analysis. Biophys Chem 286:106806. https://doi.org/10.1016/j.bpc.2022.10680

Chakri S, Frateur I, Orazem ME, Sutter E, Tran T (2017) Improved EIS analysis of the electrochemical behaviour of carbon steel in alkaline solution. Electrochim Acta 246:924–930. https://doi.org/10.1016/j.electacta.2017.06.096

Chen L, Ren S, Zhou Y, Li X, Wang M, Chen Z, Yang J (2022) Effects of doping Mn, Cu and Fe oxides on polyhedron CeO_2 catalyst during NH_3-SCR reaction. J Taiwan Inst Chem E 140 https://doi.org/10.1016/j.jtice.2022.104560

Cheng J, Xie Y, Wei Y, Xie D, Sun W, Zhang Y, Li M, An J (2021) Degradation of tetracycline hydrochloride in aqueous via

combined dielectric barrier discharge plasma and Fe-Mn doped AC. Chemosphere 286:131841. https://doi.org/10.1016/j.chemosphere.2021.131841

Cui MH, Liu WZ, Tang ZE, Cui D (2021) Recent advancements in azo dye decolorization in bio-electrochemical systems (BESs): insights into decolorization mechanism and practical application. Water Res 203:117512. https://doi.org/10.1016/j.watres.2021.117512

Fang L, Xu C, Zhang W, Huang L-Z (2018) The important role of polyvinylpyrrolidone and Cu on enhancing dechlorination of 2,4-dichlorophenol by Cu/Fe nanoparticles: performance and mechanism study. Appl Surf Sci 435:55–64. https://doi.org/10.1016/j.apsusc.2017.11.084

Gao JF, Wu ZL, Duan WJ, Zhang WZ (2019) Simultaneous adsorption and degradation of triclosan by Ginkgo biloba L. stabilized Fe/Co bimetallic nanoparticles. Sci Total Environ 662:978–989

Ge Y-L, Zhang Y-F, Yang Y, Xie S, Liu Y, Maruyama T, Deng Z-Y, Zhao X (2019) Enhanced adsorption and catalytic degradation of organic dyes by nanometer iron oxide anchored to single-wall carbon nanotubes. Appl Surf Sci 488:813–826. https://doi.org/10.1016/j.apsusc.2019.05.221

Goncalves MR, Marques IP, Correia JP (2012) Electrochemical mineralization of anaerobically digested olive mill wastewater. Water Res 46:4217–4225. https://doi.org/10.1016/j.watres.2012.05.019

Gong X, Liu Y, Wang B, Yang W, Fan L, Liu Y (2019) Nitrate reduction via micro-electrolysis on Zn-Ag bimetal combined with photo-assistance. Sci Total Environ 683:89–97. https://doi.org/10.1016/j.scitotenv.2019.05.22

Han Y, Qi M, Zhang L, Sang Y, Liu M, Zhao T, Niu J, Zhang S (2019) Degradation of nitrobenzene by synchronistic oxidation and reduction in an internal circulation microelectrolysis reactor. J Hazard Mater 365:448–456. https://doi.org/10.1016/j.jhazmat.2018.11.036

Huszánk R, Nagy G, Rajta I, Czeglédi A (2021) In-air proton beam irradiation induced radiolysis of methyl orange in aqueous solution. Radia Phys Chem 180:109322. https://doi.org/10.1016/j.radphyschem.2020.109322

Karimi-Maleh H, Beitollahi H, Senthil Kumar P, Tajik S, Mohammadzadeh Jahani P, Karimi F, Karaman C, Vasseghian Y, Baghayeri M, Rouhi J, Show PL, Rajendran S, Fu L, Zare N (2022) Recent advances in carbon nanomaterials-based electrochemical sensors for food azo dyes detection. Food Chem Toxicol 164:112961. https://doi.org/10.1016/j.fct.2022.112961

Khalakhan I, Vorokhta M, Xie X, Piliai L, Matolínová I (2021) On the interpretation of X-ray photoelectron spectra of Pt-Cu bimetallic alloys. J Electron Spectrosc 246 https://doi.org/10.1016/j.elspec.2020.147027

Khaled JM, Alyahya SA, Govindan R, Chelliah CK, Maruthupandy M, Alharbi NS, Kadaikunnan S, Issac R, Murugan S, Li WJ (2022) Laccase producing bacteria influenced the high decolorization of textile azo dyes with advanced study. Environ Res 207:112211. https://doi.org/10.1016/j.envres.2021.112211

Kishor R, Purchase D, Saratale GD, Saratale RG, Ferreira LFR, Bilal M, Chandra R, Bharagava RN (2021) Ecotoxicological and health concerns of persistent coloring pollutants of textile industry wastewater and treatment approaches for environmental safety. J Environ Chem Eng 9 https://doi.org/10.1016/j.jece.2020.105012

Li P-N, Ghule AV, Chang J-Y (2017a) Direct aqueous synthesis of quantum dots for high-performance AgInSe 2 quantum-dot-sensitized solar cell. J Power Sources 354:100–107. https://doi.org/10.1016/j.jpowsour.2017.04.040

Li P, Liu Z, Wang X, Guo Y, Wang L (2017b) Enhanced decolorization of methyl orange in aqueous solution using iron-carbon micro-electrolysis activation of sodium persulfate. Chemosphere 180:100–107. https://doi.org/10.1016/j.chemosphere.2017.04.019

Liu Y, Wang C, Sui Z, Zou D (2018) Degradation of chlortetracycline using nano micro-electrolysis materials with loading copper. Sep Purif Technol 203:29–35. https://doi.org/10.1016/j.seppur.2018.03.064

Liu J, Su J, Ali A, Wang Z, Chen C, Xu L (2021) Role of porous polymer carriers and iron-carbon bioreactor combined micro-electrolysis and biological denitrification in efficient removal of nitrate from wastewater under low carbon to nitrogen ratio. Bioresour Technol 321:124447. https://doi.org/10.1016/j.biortech.2020.124447

Luo S, Yang, Wang X, Sun C (2010) Reductive degradation of tetrabromobisphenol A over iron-silver bimetallic nanoparticles under ultrasound radiation. Chemosphere. https://doi.org/10.1016/j.chemosphere.2010.02.011

Ma C, Ran Z, Yang Z, Wang L, Wen C, Zhao B, Zhang H (2019) Efficient pretreatment of industrial estate wastewater for biodegradability enhancement using a micro-electrolysis-circulatory system. J Environ Manage 250:109492. https://doi.org/10.1016/j.jenvman.2019.109492

Miao F, Liu Z, Kang X, Cheng C, Mao X, Li R, Lin H, Zhang H (2021) Electro-enhanced heterogeneous activation of peroxymonosulfate via acceleration of Fe(III)/Fe(II) redox cycle on Fe-B catalyst. Electrochim Acta 377:138073. https://doi.org/10.1016/j.electacta.2021.138073

Niu H, He D, Yang Y, Lv H, Liang Y (2019) Long-lasting activity of Fe0-C internal microelectrolysis-Fenton system assisted by Fe@C-montmorillonites nanocomposites. Appl Catal B-Environ 256:117820. https://doi.org/10.1016/j.apcatb.2019.117820

Panimalar S, Chandrasekar M, Logambal S, Uthrakumar R, Inmozhi C (2022) Europium-doped MnO_2 nanostructures for controlling optical properties and visible light photocatalytic activity. Mater Today: Proc 56:3394–3401. https://doi.org/10.1016/j.matpr.2021.10.335

Paparazzo E (2017) On the number, binding energies, and mutual intensities of Ce3d peaks in the XPS analysis of cerium oxide systems: a response to Murugan et al., Superlatt. Microstruct. 85 (2015) 321. Superlattice Microst 105:216–2020. https://doi.org/10.1016/j.spmi.2016.06.025

Peng C, Chen L, Wu X, Wei X, Tehrim A, Dai M, Xu S (2021) Identification of adsorption or degradation mechanism for the removal of different ionic dyes with iron-carbon micro-electrolysis process. J Environ Chem Eng 9 https://doi.org/10.1016/j.jece.2021.105690

Pete S, Kattil RA, Thomas L (2021) Polyaniline-multiwalled carbon nanotubes (PANI- MWCNTs) composite revisited: an efficient and reusable material for methyl orange dye removal. Diam Relat Mat. https://doi.org/10.1016/j.diamond.2021.108455

Qiang H, Wen L, Peng P, Huang W (2013) Reductive debromination of tetrabromobisphenol A by Pd/Fe bimetallic catalysts. Chemosphere 92:1321–1327. https://doi.org/10.1016/j.chemosphere.2013.05.021

Ravinuthala S, Nair AV, Sharma N, Lokesh S, Madhusudhan MC, Das SP (2022) Co-substrates' influence on bioelectricity production in an azo dye-based microbial fuel cell. Bioresource Technol Reports 18. https://doi.org/10.1016/j.biteb.2022.101012

Rubeena KK, Hari Prasad Reddy P, Laiju AR, Nidheesh PV (2018) Iron impregnated biochars as heterogeneous Fenton catalyst for the degradation of acid red 1 dye. J Environ Manage 226:320–328. https://doi.org/10.1016/j.jenvman.2018.08.055

Segura Y, Martínez F, Melero JA (2013) Effective pharmaceutical wastewater degradation by Fenton oxidation with zero-valent iron. Appl Catal B-Environ 136–137:64–69. https://doi.org/10.1016/j.apcatb.2013.01.036

Shen Y, Zhao Q, Li X, Hou Y (2021) Comparative investigation of visible-light-induced benzene degradation on M-ferrite/hematite (M = Ca, Mg, Zn) nanospheres by in situ FTIR: intermediates and

reaction mechanism. Colloid Surface A 618:126501. https://doi.org/10.1016/j.colsurfa.2021.126501

Si Z, Song X, Wang Y, Cao X, Wang Y, Zhao Y, Ge X, Sand W (2020) Untangling the nitrate removal pathways for a constructed wetland- sponge iron coupled system and the impacts of sponge iron on a wetland ecosystem. J Hazard Mater 393:122407. https://doi.org/10.1016/j.jhazmat.2020.122407

Sun L, Mo Y, Zhang L (2022) A mini review on bio-electrochemical systems for the treatment of azo dye wastewater: state-of-the-art and future prospects. Chemosphere 294:133801. https://doi.org/10.1016/j.chemosphere.2022.133801

Wang L, Yang Q, Wang D, Li X, Zeng G, Li Z, Deng Y, Liu J, Yi K (2016) Advanced landfill leachate treatment using iron-carbon microelectrolysis- Fenton process: process optimization and column experiments. J Hazard Mater 318:460–467. https://doi.org/10.1016/j.jhazmat.2016.07.033

Wang J, Zhang Q, Shao X, Ma J, Tian G (2018) Properties of magnetic carbon nanomaterials and application in removal organic dyes. Chemosphere 207:377–384. https://doi.org/10.1016/j.chemosphere.2018.05.109

Wu Xiaoyan, Lv Chunxue, Yu Shoufu, Li Mi, Ye Jian, Zhang Xiaowen, Liu Yong (2020) Uranium (VI) removal from aqueous solution using iron-carbon micro-electrolysis packing. Separation and Purification Technology 234:116104. https://doi.org/10.1016/j.seppur.2019.116104

Xia Q, Zhang D, Yao Z, Jiang Z (2021) Investigation of Cu heteroatoms and Cu clusters in Fe-Cu alloy and their special effect mechanisms on the Fenton-like catalytic activity and reusability. Appl Catal B-Environ 299. https://doi.org/10.1016/j.apcatb.2021.120662

Xie HN, Li J, Wang YE, Zhao W, Li J (2021) Influencing factors for the Fenton-like of biological sponge iron system and its degradation mechanism of aniline. Process Biochem 101:230–236. https://doi.org/10.1016/j.procbio.2020.11.012

Xu WY, Gao TY, Fan JH (2005) Reduction of nitrobenzene by the catalyzed Fe-Cu process. J Hazard Mater 123:232–241. https://doi.org/10.1016/S1001-0742(08)62186-5

Xu Z, Sun Z, Zhou Y, Zhang D, Chen W (2019) Enhanced hydrodechlorination of p-chloronitrobenzene by a GAC-Fe-Cu ternary micro-electrolysis system: synergistic effects and removal mechanism. Sep Purif Technol 237:116391. https://doi.org/10.1016/j.seppur.2019.116391

Yamaguchi R, Kurosu S, Suzuki M, Kawase Y (2018) Hydroxyl radical generation by zero-valent iron/Cu (ZVI/Cu) bimetallic catalyst in wastewater treatment: heterogeneous Fenton/Fenton-like reactions by Fenton reagents formed in-situ under oxic conditions. Chem Eng J 334:1537–1549. https://doi.org/10.1016/j.cej.2017.10.154

Yu Y, Huang Z, Deng D, Ju Y, Ren L, Xiang M, Li L, Li H (2017a) Synthesis of millimeter-scale sponge Fe/Cu bimetallic particles removing TBBPA and insights of degradation mechanism. Chem Eng J 325:279–288. https://doi.org/10.1016/j.cej.2017.05.018

Yu Y, Zheng H, Deng D, Ju Y, Hui L (2017b) Synthesis of millimeter-scale sponge Fe/Cu bimetallic particles removing TBBPA and insights of degradation mechanism. Chem Eng J 325:279–288. https://doi.org/10.1016/j.cej.2017.05.018

Yu Y, Huo H, Zhang Q, Chen Y, Wang S, Liu X, Chen C, Min D (2022) Nano silver decorating three-dimensional porous wood used as a catalyst for enhancing azo dyes hydrogenation in wastewater. Ind Crop Prod 175. https://doi.org/10.1016/j.indcrop.2021.114268

Zhang J, Ren L, Zhang D, Li J, Peng S, Han X, Ding A, Lu P (2019) Reduction of NO to N_2 in an autotrophic up-flow bioreactor with sponge iron bed based Fe(II)EDTA complexation. Fuel 254. https://doi.org/10.1016/j.fuel.2019.115631

Zhao H, Nie T, Zhao H, Liu Y, Zhang J, Ye Q, Xu H, Shu S (2021) Enhancement of Fe-C micro-electrolysis in water by magnetic field: mechanism, influential factors and application effectiveness. J Hazard Mater 410:124643. https://doi.org/10.1016/j.jhazmat.2020.124643

Zheng Z, Yuan S, Liu Y, Lu X, Wan J, Wu X, Chen J (2009) Reductive dechlorination of hexachlorobenzene by Cu/Fe bimetal in the presence of nonionic surfactant. J Hazard Mater 170:895–901. https://doi.org/10.1016/j.jhazmat.2009.05.052